NEUROSCIENCE

Specialized cutaneous Schwann cells initiate pain sensation

Hind Abdo[1]*, Laura Calvo-Enrique[1]*, Jose Martinez Lopez[1], Jianren Song[2], Ming-Dong Zhang[1], Dmitry Usoskin[1], Abdeljabbar El Manira[2], Igor Adameyko[3], Jens Hjerling-Leffler[1], Patrik Ernfors[1]†

An essential prerequisite for the survival of an organism is the ability to detect and respond to aversive stimuli. Current belief is that noxious stimuli directly activate nociceptive sensory nerve endings in the skin. We discovered a specialized cutaneous glial cell type with extensive processes forming a mesh-like network in the subepidermal border of the skin that conveys noxious thermal and mechanical sensitivity. We demonstrate a direct excitatory functional connection to sensory neurons and provide evidence of a previously unknown organ that has an essential physiological role in sensing noxious stimuli. Thus, these glial cells, which are intimately associated with unmyelinated nociceptive nerves, are inherently mechanosensitive and transmit nociceptive information to the nerve.

The ability to detect and protect from damage-causing (noxious) stimuli relies on the existence of sensory afferents, called nociceptors (*1*–*6*). Nociceptive nerves are generally unmyelinated and associate with Remak glial cells that protect and metabolically support the axons (*7*, *8*). The unmyelinated nerve endings are activated by noxious stimuli and, hence, represent the pain receptors in the skin. We used genetic labeling to address how cutaneous glia (Schwann cells) distribute and interact with nociceptive nerve terminals. Neural-crest and glia-specific Cre lines (Plp-CreERT2, Sox10-CreERT2, Sox2-CreERT2) coupled to the Rosa26-enhanced YFP ($R26R^{YFP}$) or $R26R^{tdTOMATO}$ ($R26R^{TOM}$) reporter lines were used. Recombination in Schwann cells and staining for nerves with PGP9.5 revealed cutaneous Schwann cells in a static location in the dermis, close to the dermal/epidermal border in both glabrous and hairy skin, and were closely associated with ascending nerve fibers in both Plp-YFP (Fig. 1A and fig. S1, A and C) and Sox10-TOM mice. The latter also revealed epidermal Schwann cell processes attached to nerves, likely because of brighter fluorescence (Fig. 1B and fig. S1, B and D). Consistent with Schwann cells, these were Plp^{YFP+}, $SOX10^{+}$, and $S100\beta^{+}$ cells with extensive radial processes into epidermis (Fig. 1A). Transmission electron microscopy revealed that nerve terminals emerged from the soma of Schwann cells located a few micrometers from the border to epidermis with the glia as the only source of cytoplasmic sheaths. Ascending immediate subepidermis nerves branched with radial Schwann cell processes, ensheathing progressively fewer nerves. In intraepidermal endings, smaller parts of nerve terminals were in contact with glia processes (Fig. 1C and fig. S2A). Nerve and Schwann cell processes were surrounded by a thick layer of fibrillar collagen oriented in the direction of the glio-neural complex and distinct from the rest of collagen. These morphologically distinct glia also carried high expression of Aquaporin1 (Fig. 1E) and were associated with $CGRP^{+}$, $P2RX3^{+}$, and transient receptor potential $V1^{+}$ nociceptive fibers (Fig. 1F and fig. S2B). Immunoelectron microscopy for TOMATO in Sox10-TOM mice confirmed Tomato

[1]Department of Medical Biochemistry and Biophysics, Division of Molecular Neurobiology, Karolinska Institutet, Stockholm 17177, Sweden. [2]Department of Neuroscience, Karolinska Institutet, Stockholm 17177, Sweden. [3]Department of Physiology and Pharmacology, Karolinska Institutet, Stockholm 17177, Sweden.
*These authors contributed equally to this work.
†Corresponding author. Email: patrik.ernfors@ki.se

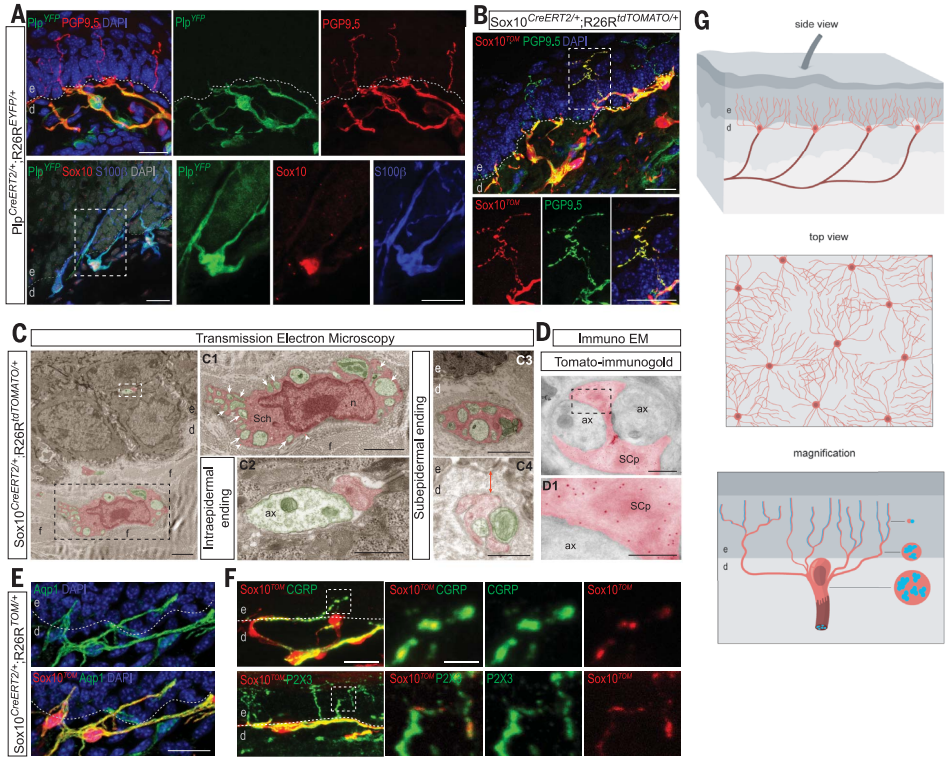

Fig. 1. Cutaneous Schwann cells form a glio-neural end organ in the skin. (**A** and **B**) Cutaneous Schwann cells in the subepidermal border with radial processes into epidermis ensheath unmyelinated nerve endings. Genetically labeled Schwann cells in Plp-YFP (A) and Sox10-TOM (B) mice associate with unmyelinated nerves ($PGP9.5^{+}$) and express glia markers SOX10 and S100β. Insets show higher magnification. (**C** and **D**) Transmission electron microscopy of the glio-neural complex. Images were pseudo-colored (axons, green and cutaneous Schwann cell and its processes, red). (C1) Subepidermal border and (C2) epidermis are higher magnification of boxed area in (C). Arrowheads point to basal lamina on the abaxonal surface, and arrows point to axons. (C3 and C4) Subepidermal Schwann cell processes enfold few (C4) or several axons (C3) close to the epidermis (red arrow is 1 μm in C4). (D) Immuno–electron microscopy (EM) with anti-dsRed antibody (red dots) shows specific expression of TOMATO in Schwann cell process and not by the axons. (**E**) Immunohistochemistry for Aquaporin1 (Aqp1). (**F**) Immunohistochemistry for CGRP and P2X3. (**G**) Schematic illustration of the glio-neural complex in the subepidermal border and epidermis (nociceptive Schwann cell, red and nerves, blue). Hatched line indicates dermal-epidermal border. ax, axon; d, dermis; DAPI, 4′,6-diamidino-phenylindole; e, epidermis; f, fibrillar collagen; n, nucleus; Sch, cutaneous Schwann cell; SCp, Schwann cell process.

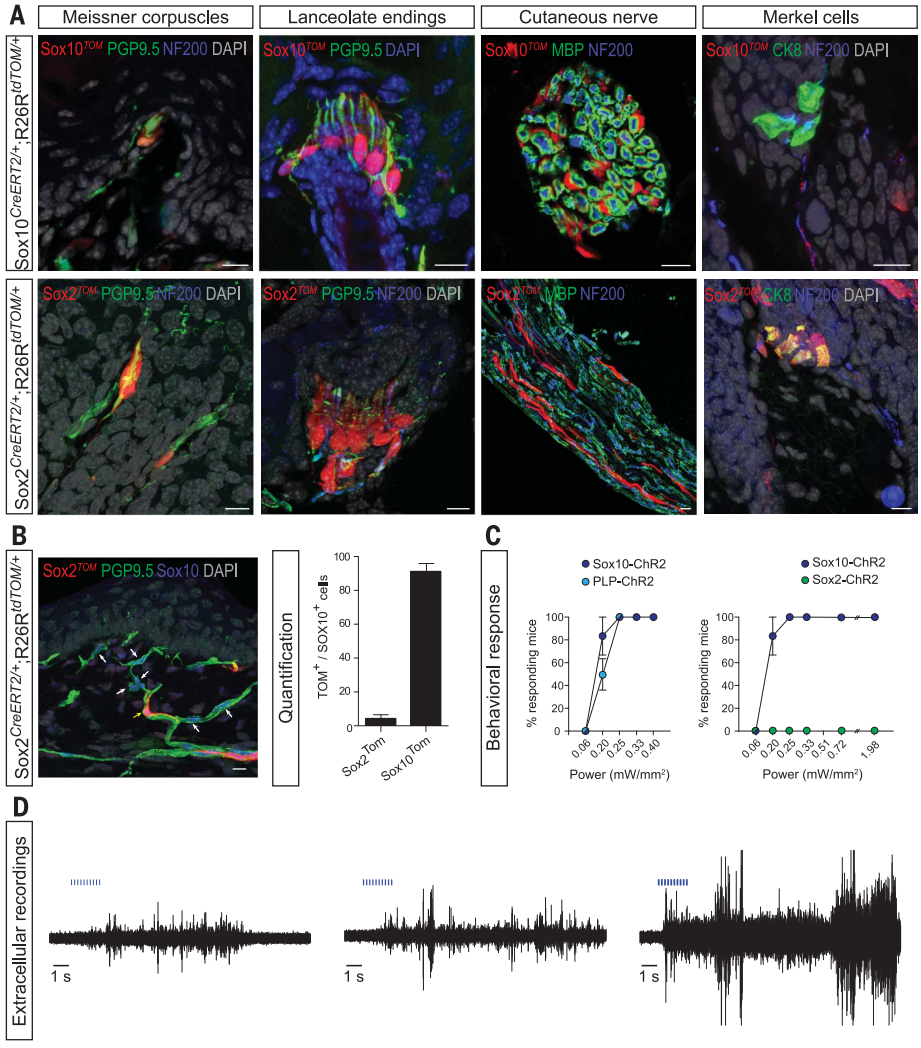

Fig. 2. Nociceptive Schwann cells can initiate pain-like behavior and are sufficient to elicit action potential propagation. (**A**) Immunohistochemistry reveals recombination in LTMR end-organ glia and in Remak glia of nerves in Sox10-TOM and Sox2-TOM mice, and in the latter also in Merkel cells. (**B**) Sox10-TOM but rarely Sox2-TOM mice recombine in nociceptive Schwann cells ($SOX10^+$). White arrows indicate non-recombined and yellow arrow indicates occasional recombined $SOX10^+$ Schwann cell in Sox2-TOM mice. Quantification is on right. (**C**) Optogenetic stimulation of nociceptive Schwann cells results in nocifensive behavior. Sox10-ChR2 and Plp-ChR2 mice but not Sox2-ChR2 mice respond to blue-light application. (**D**) Activation of nociceptive Schwann cells results in nerve electrical activity. Extracellular recording from the palmar nerve after optogenetic stimulation (blue marks) of the skin in Sox10-ChR2 mice. MBP, myelin basic protein; NF200, neurofilament 200.

in ultrastructurally identified glial cells (Fig. 1D and fig. S2C). Thus, a morphologically and molecularly specialized type of Schwann cells (hereafter termed nociceptive Schwann cells) form a mesh-like network in the subepidermal border that constructs a glio-neural complex through an intimate association with nociceptive nerves (Fig. 1G, schematic illustration) that is insulated by structural support of collagen fibers.

To determine whether nociceptive Schwann cells contribute to pain perception, we first analyzed recombination in various glia compartments of Plp-YFP, Sox10-TOM, and Sox2-TOM mice. Both Plp-YFP and Sox10-TOM mice recombine in nociceptive Schwann cells and terminal Schwann cells of Meissner corpuscles, lanceolate endings, and glia in nerves but not Merkel cells or dorsal root ganglion neurons (Fig. 2A and fig. S3). By contrast, Sox2-TOM mice largely failed to recombine nociceptive Schwann cells (Fig. 2B) but recombined in all other compartments seen for Sox10-TOM as well as Merkel cells (Fig. 2A and fig. S4). Thus, if crossed to light-sensitive channels, these driver strains can be used to manipulate Schwann cell activity without direct stimulation of sensory nerves and thereby resolve the role of nociceptive versus other cutaneous Schwann cell types.

The driver strains were crossed to Channelrhodopsin-2 (ChR2)–enhanced YFP mice to generate Plp-ChR2 and Sox10-ChR2 mice. We wanted to determine whether optogenetic stimulation of nociceptive Schwann cells is sufficient to elicit pain-like responses. A light power–dependent increase in limb withdrawal was observed in both strains (Fig. 2C). Extracellular recording from the palmar nerve after light stimulation of the palmar skin revealed increased firing with increased length of light pulses (1, 10, or 50 ms), including C-fiber mass activity and maybe also A-fiber high-amplitude bursts (Fig. 2D). The low-threshold mechanoreceptors (LTMRs) terminating as lanceolate endings in hair follicles and innervating Merkel cells and Meissner corpuscles elicit sensations of hair deflection, touch, pressure, flutter, or vibration but not pain behavior (*9*). However, in chronic pain, light touch–activated neurons can contribute to mechanical allodynia (*10*–*12*). In contrast with Sox10-ChR2 positive control mice that displayed a robust light intensity–dependent response, optogenetic stimulation of LTMR terminal Schwann cells in Sox2-ChR2 mice failed to evoke a withdrawal response (Fig. 2C) and therefore do not contribute to the withdrawal response.

To ascertain that the reflexive defensive responses are caused by pain, we assayed coping behavior that may serve to soothe suffering (*13*). Optogenetic stimulation led to robust licking, shaking, and paw-guarding behavior (Fig. 3A).

To resolve the sensory modalities nociceptive Schwann cells modulate, optogenetic activation that is subthreshold to elicit behavior was combined with cold, heat, and mechanical stimuli. We reasoned that coincident subthreshold light could sensitize to the physiological stimuli that it modulates. Coping-behavior subthreshold stimulation significantly increased sharp 2-g von Frey coping behavior, whereas paw-withdrawal subthreshold stimuli did not affect touch sensitivity, measured by the cotton swab withdrawal assay (*14*) (Fig. 3, B and C), although they elevated the response to cold stimuli in both Plp-ChR2 and Sox10-ChR2 mice (Fig. 3, D and E, and fig. S5, B and C). In Sox10-ArchT mice generated to silence nociceptive Schwann cells, no difference in cold response was seen (Fig. 3F and fig. S5D). Withdrawal subthreshold optogenetic stimulation in Plp-ChR2 and Sox10-ChR2 potentiated heat-evoked

responses (Fig. 3, G and H, and fig. S5, A and E), but silencing did not result in any difference of the thermal threshold (Fig. 3I and fig. S5F). Plp-ChR2 mice displayed dose-dependent reduction of the mechanical withdrawal threshold by increasing the length of subthreshold light trains (Fig. 3J), confirmed in Sox10-ChR2 mice after coincident activation of Schwann cells (Fig. 3K and fig. S5G). Unlike for cold and heat, silencing resulted in a significantly increased mechanical threshold, which was reversed after 24 hours (Fig. 3L and fig. S5H).

Electrical properties of nociceptive Schwann cells were examined in dissociated Sox10-TOM–expressing nociceptive Schwann cells by whole-cell current-clamp electrophysiological recordings. Stepwise current injections revealed two-phase linear I-V relationships around the resting membrane potential (Fig. 4, A and B), with a clear knee precisely around their resting membrane potential (average of −32.56 ± 1.36 mV) (Fig. 4C). The decreased resistance upon depolarization (Fig. 4, D and E) indicates an intrinsic (nonmechanical) opening of channels, pulling the membrane potential toward resting value. The passive membrane properties indicated a slow time constant, within the range of neurons (Fig. 4F).

We measured electrical responses to mechanical stimuli to determine whether nociceptive Schwann cells are mechanically active. Whole-cell voltage response to mechanical force in steps of 40 nm with five or 10 steps at ~60 Hz, a pause, and thereafter five or 10 steps out was measured. Mechanical stimulation produced a transient depolarization (n = 9) (Fig. 4, G and H). Four cells did not return all the way to baseline, possibly because of the mechanical force affecting the integrity of the seal. In the remaining cells, the decay was essentially complete during continued force application, suggesting that the mechanoreceptive response adapts to sustained force over time. Both response and adaptation were very rapid, resulting in similar responses in the subsequent stimuli. The cells tracked the maximum frequency of stimuli that we could generate (60 Hz). Releasing the force also depolarized the cells (Fig. 4G). Thus, nociceptive Schwann cells responded to both positive and negative changes in force but much less to sustained force. Peak mean amplitude was 25.5 ± 2.1 mV (Fig. 4I), and 50% depolarization duration (half-width) was 6.7 ± 1.5 ms (Fig. 4J), with time at the beginning of the rising phase to the peak (rise time) of 1.4 ± 0.2 ms (Fig. 4K). This time course of the mechanoreceptor potential may reflect that of the underlying mechanoreceptor current. This suggests very fast gating mechanisms, similar to what has been described in sensory neurons (*15*, *16*).

We provide evidence for a specialized glial cell type that builds a sensory organ in the skin, initiating the sensation of pain. The nociceptive Schwann cells display a mesh-like network of cytoplasmic sheaths around nerves in the subepidermal border with radial processes entering into the epidermis abutting to unmyelinated nociceptive nerves. The nociceptive Schwann cells are the cellular equivalents of the ignored Remak Schwann

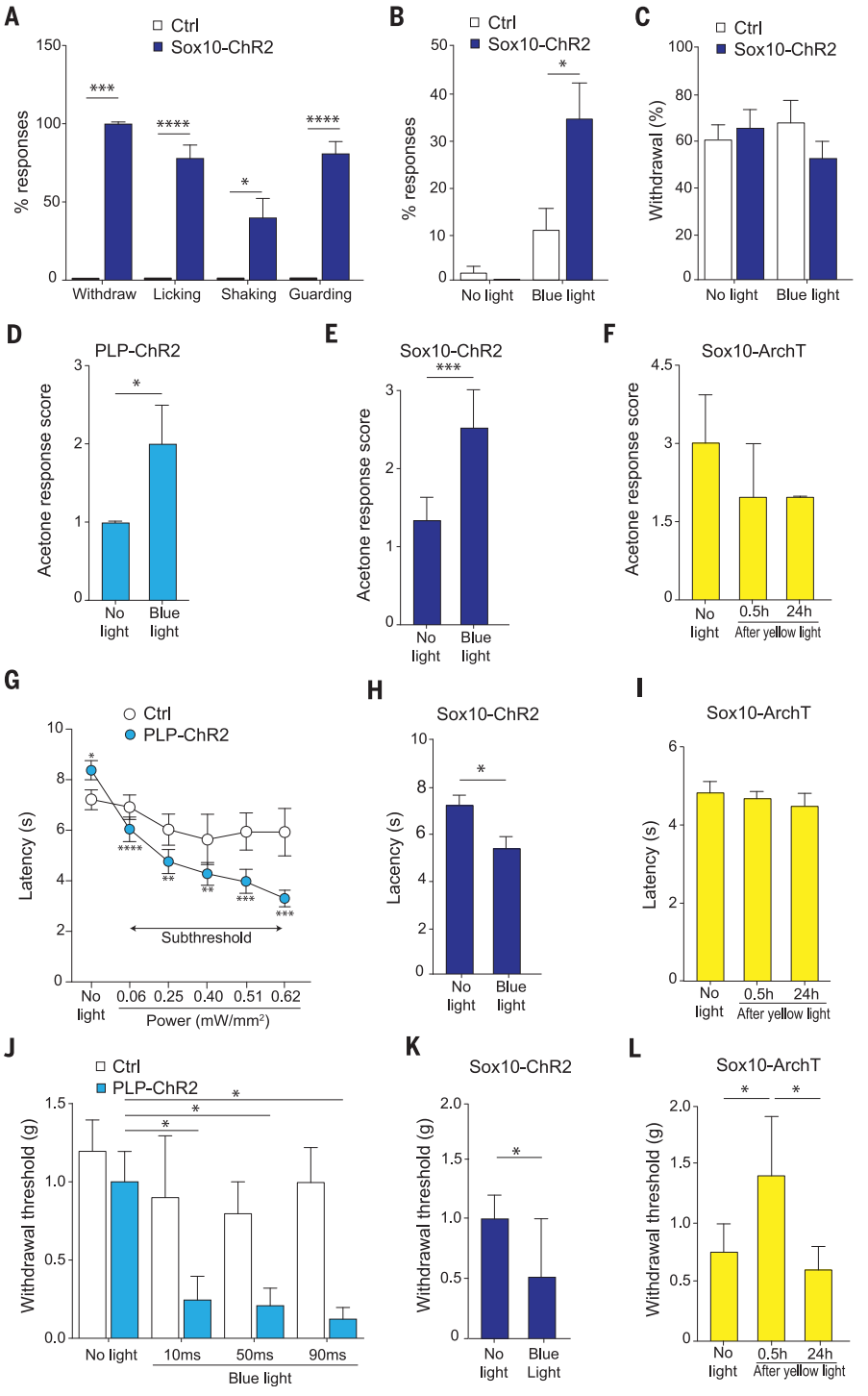

Fig. 3. Nociceptive Schwann cells determine the sensitivity threshold for mechanosensation. (**A**) Suprathreshold photoactivation of nociceptive Schwann cells evokes coping behavior associated with pain. (**B** to **L**) Blue bars, subthreshold optogenetic activation of nociceptive Schwann cells combined with natural stimuli and yellow bars before and after optogenetic inhibition. (B) Coping response to nociceptive mechanical stimuli (2-g von Frey). (C) Withdrawal to cotton swab. (D to F) Response to cold. (G to I) Withdrawal latency to heat. (J) Mechanical threshold without light or with increased length of subthreshold blue-light trains. (K) Mechanical threshold. (L) Mechanical threshold before or after optogenetic inhibition. Ctrl, control. Statistics text and *P* values can be found in the supplementary materials, material and methods.

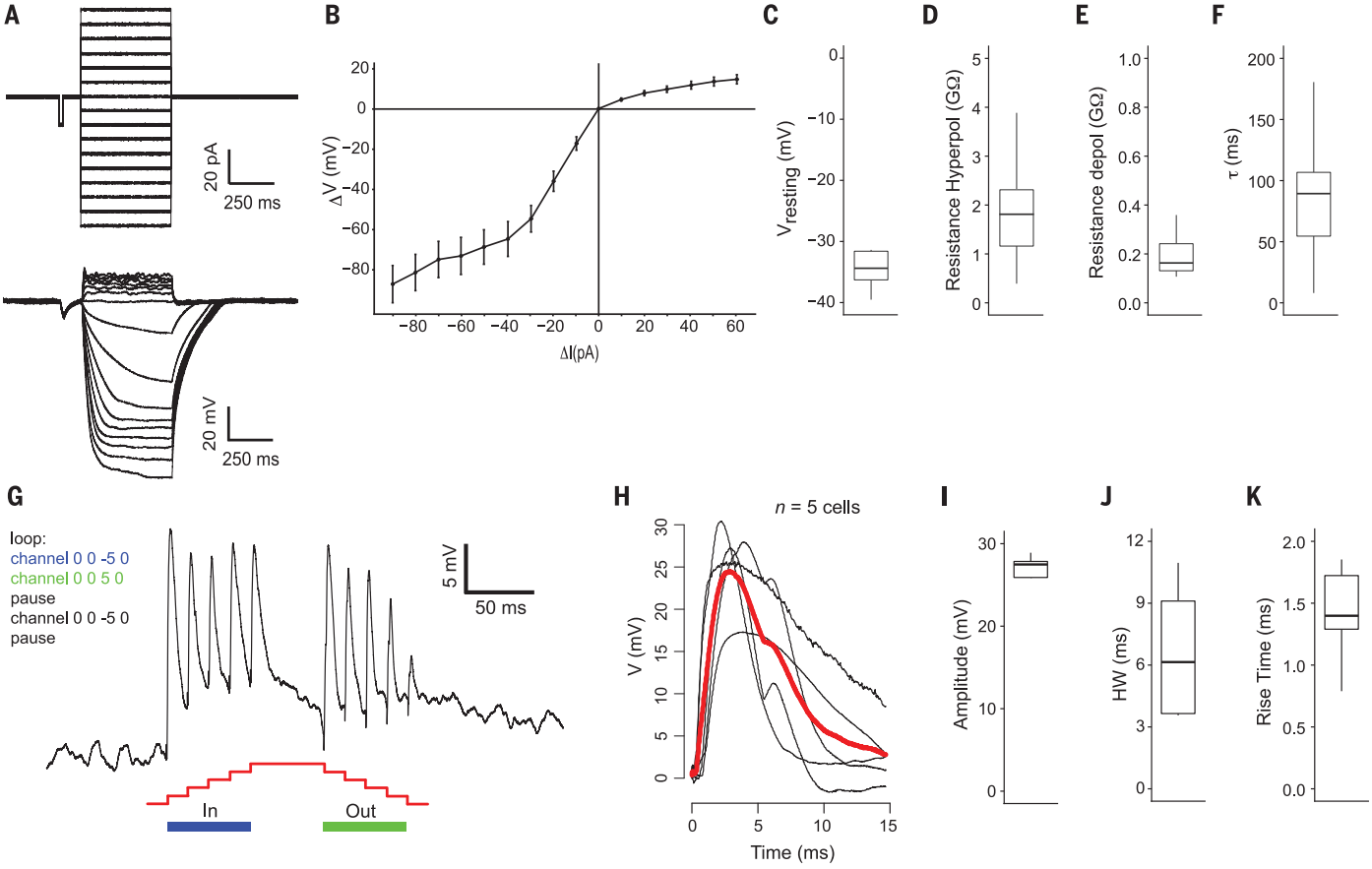

Fig. 4. Nociceptive Schwann cells are mechanosensory cells. (**A**) Voltage signal detected during whole-cell current-clamp recordings evoked current steps. (**B**) Two-phase linear I-V relationships during hyperpolarization and depolarization. (**C**) Resting membrane potential of nociceptive Schwann cells. (**D**) Resistance of cells calculated during hyperpolarizing current injections. (**E**) Resistance of cells calculated during depolarizing current injections. (**F**) Time constant (τ). (**G**) Mechanical stimulation of nociceptive Schwann cells during whole-cell current-clamp recordings; example of inward steps and subsequent outward steps applied as indicated. (**H**) Mechanically evoked depolarization (red, average). (**I**) Amplitudes of depolarization. (**J**) Half-width of depolarization. (**K**) 10 to 90% rise time of the depolarization. depol, depolarization; HW, half-width; Hyperpol, hyperpolarization.

cells described in the subepidermal border of the skin some 45 years ago. At that time, nerve fibers were thought to lose their glia attachment and enter epidermis as free nerve endings (*17*). The nociceptive Schwann cells are highly mechanosensitive with rapid adaptation and respond to both positive and negative changes in force, similar to "on" and "off" mechanoreceptor responses observed in *Caenorhabditis elegans* (*18*). They transduce nociceptive stimuli into electrical signals that translate into pain-like behavior. The nociceptive nerve endings in skin also gate responses to various noxious stimuli (*1*–*6*). Hence, nociceptive nerves and nociceptive Schwann cells form a nociceptive glio-neural complex with two sensor-receptor cell types, the glia and the nerve, both likely influencing the sensation of pain. Most or all types of nociceptors appear to contribute to the nociceptive glio-neural complex, and consistently, both mechanical and thermal nociception is potentiated in gain-of-function experiments. However, loss-of-function experiments indicate either that activation of thermosensitive ion channels in primary afferents (*19*–*22*) is sufficient by itself or, alternatively, that nociceptive Schwann cells contribute to a submodality not captured in our behavioral tests. By contrast, nociceptive Schwann cells are physiologically contributing to sensation of mechanical stimuli, as the threshold was affected in both gain- and loss-of-function experiments. This could suggest a broader response profile of discrete nociceptive neuron types than that predicted from their molecular profiles (*23*–*26*). Functional implications of our findings are vast if nerve and glial cell receptor types mediate different aspects of thermal and mechanical nociceptive transduction, as has been proposed for Merkel cells participating in non-noxious touch sensation (*27*–*29*).

REFERENCES AND NOTES

1. V. E. Abraira, D. D. Ginty, *Neuron* **79**, 618–639 (2013).
2. M. Costigan, J. Scholz, C. J. Woolf, *Annu. Rev. Neurosci.* **32**, 1–32 (2009).
3. F. Lallemend, P. Ernfors, *Trends Neurosci.* **35**, 373–381 (2012).
4. Y. Liu, Q. Ma, *Curr. Opin. Neurobiol.* **21**, 52–60 (2011).
5. C. Peirs *et al.*, *Neuron* **87**, 797–812 (2015).
6. S. A. Prescott, Q. Ma, Y. De Koninck, *Nat. Neurosci.* **17**, 183–191 (2014).
7. B. L. Harty, K. R. Monk, *Curr. Opin. Neurobiol.* **47**, 131–137 (2017).
8. K. R. Jessen, R. Mirsky, *J. Physiol.* **594**, 3521–3531 (2016).
9. C. J. Woolf, T. P. Doubell, *Curr. Opin. Neurobiol.* **4**, 525–534 (1994).
10. R. Dhandapani *et al.*, *Nat. Commun.* **9**, 1640 (2018).
11. M. Koltzenburg, L. E. Lundberg, H. E. Torebjörk, *Pain* **51**, 207–219 (1992).
12. C. Peng *et al.*, *Science* **356**, 1168–1171 (2017).
13. T. Huang *et al.*, *Nature* **565**, 86–90 (2019).
14. S. S. Ranade *et al.*, *Nature* **516**, 121–125 (2014).
15. K. Poole, R. Herget, L. Lapatsina, H. D. Ngo, G. R. Lewin, *Nat. Commun.* **5**, 3520 (2014).
16. Y. Song *et al.*, *J. Physiol. Biochem.* **74**, 207–221 (2018).
17. N. Cauna, *J. Anat.* **115**, 277–288 (1973).
18. R. O'Hagan, M. Chalfie, M. B. Goodman, *Nat. Neurosci.* **8**, 43–50 (2005).
19. M. J. Caterina *et al.*, *Nature* **389**, 816–824 (1997).
20. D. D. McKemy, W. M. Neuhausser, D. Julius, *Nature* **416**, 52–58 (2002).
21. A. M. Peier *et al.*, *Cell* **108**, 705–715 (2002).
22. I. Vandewauw *et al.*, *Nature* **555**, 662–666 (2018).
23. C. Li, S. Wang, Y. Chen, X. Zhang, *Neurosci. Bull.* **34**, 200–207 (2018).
24. C. L. Li *et al.*, *Cell Res.* **26**, 83–102 (2016).
25. D. Usoskin *et al.*, *Nat. Neurosci.* **18**, 145–153 (2015).
26. A. Zeisel *et al.*, *Cell* **174**, 999–1014.e22 (2018).
27. R. Ikeda *et al.*, *Cell* **157**, 664–675 (2014).

28. S. Maksimovic *et al*., *Nature* **509**, 617–621 (2014).
29. S. H. Woo *et al*., *Nature* **509**, 622–626 (2014).

ACKNOWLEDGMENTS

We thank M. Karlén for schematic illustrations. **Funding**: P.E. received the ERC (PainCells 740491), the Swedish MRC, KAW Scholar and project grant, and Welcome Trust (200183). M.-D.Z. received a brain foundation post-doc fellowship. **Author contributions**: Conceptualization: P.E. and I.A.; mouse models/behavior/experimental design: H.A. and L.C.-E.; electrophysiology: J.M.L. and J.H.-L.; nerve recording: J.S. and A.E.M.; Immuno: H.A., L.C.-E., and M.-D.Z.; animal platforms: D.U.; writing (H.A., L.C.-E., and P.E.) and revision (L.C.-E. and P.E.) of the manuscript with input from all authors: L.C.-E. and P.E.; and supervision and funding: P.E. **Competing interests**: No competing interests. **Data and materials availability:** All data are available in the manuscript or the supplementary material. The Sox10-CreERT2 mice were obtained under an MTA from MRC.

SUPPLEMENTARY MATERIALS

science.sciencemag.org/content/365/6454/695/suppl/DC1
Materials and Methods
Supplementary Text
Figs. S1 to S5

10 April 2019; accepted 2 July 2019
10.1126/science.aax6452